Russian Journal *of* Earth Sciences Online ISSN: 1681-1208

Special Issue: "Kamchatka Earthquake M 8.8 on July 29, 2025"

Using Open GNSS Stations to Determine Earth Surface Displacements and Ionospheric Response Following the Kamchatka Earthquake of July 29, 2025

R. V. Zagretdinov[1,*], **V. F. Bakhtiarov**[1], **V. V. Kalinnikov**[2], **D. A. Kogogin**[1], **D. S. Maksimov**[1], **I. A. Nasyrov**[1], and **A. A. Zagretdinov**[1]

[1]Kazan (Volga Region) Federal University, Kazan, Russian Federation
[2]Innopolis University, Innopolis, Russian Federation
* **Correspondence to:** Renat Zagretdinov, Renat.Zagretdinov@kpfu.ru

Abstract: This study analyzes crustal movements and ionospheric response triggered by the powerful M_W 8.8 earthquake of July 29, 2025, using continuous GNSS observations from open geodetic network stations located on the Kamchatka Peninsula, Sakhalin Island, the coast of the Sea of Okhotsk, and the Kuril Islands. Significant coseismic horizontal and vertical coordinate changes were detected at GNSS stations on the Kamchatka Peninsula near Petropavlovsk-Kamchatsky (up to 65 cm horizontally and 8 cm vertically), in Severo-Kurilsk city (168 cm horizontally and 19 cm vertically), and on Sakhalin Island (up to 3 cm horizontally). The time delay of surface deformation propagation was estimated for stations in Petropavlovsk-Kamchatsky and Severo-Kurilsk. The ionospheric response to the earthquake was investigated, revealing concentric ionospheric disturbances propagating southwestward from the earthquake epicenter. Two modes of this disturbance were identified: a fast mode with a propagation velocity of 800–1300 m/s detectable during the first ~20 minutes, and a slow mode with velocity of 180–330 m/s observed approximately 40 minutes after the main shock.

Keywords: Aftershock displacements, surface movements, Precise Point Positioning (PPP), InnoGNSS, Total Electron Content (TEC), Kamchatka megathrust earthquake

Citation: Zagretdinov R. V., Bakhtiarov V. F., Kalinnikov V. V., Kogogin D. A., Maksimov D. S., Nasyrov I. A., and Zagretdinov A. A. (2026), Using Open GNSS Stations to Determine Earth Surface Displacements and Ionospheric Response Following the Kamchatka Earthquake of July 29, 2025, *Russian Journal of Earth Sciences*, 26, ES2022, EDN: VTIVBR, https://doi.org/10.2205/2026es001132

Research Article

Received: February 2, 2026
Accepted: May 25, 2026
Published: July 1, 2026

1. Introduction

The "Center for Geodesy, Cartography, and Spatial Data Infrastructure" provides information about stations of the Fundamental Astronomical and Geodetic Network (FAGN, https://rgs.cgkipd.ru/) and the Federal Geodetic Stations Network (FGSN, https://fsgs.cgkipd.ru/) [*Lapshin and Staroverov*, 2024]. As of October 2025, the organization's websites contain information about 3,190 FGSN stations belonging to regional and commercial operators of high-precision GNSS networks, and 112 stations of the state geodetic network FAGN. Measurement information from FGSN stations is available from station owners on a commercial or free basis, while coordinates and RINEX files of the FAGN network are publicly accessible (on the website).

At Kazan (Volga Region) Federal University, an automated system for collecting and processing GLONASS/GPS measurements has been operating for more than ten years, covering nearly 2,000 stationary GNSS stations across Russia, most of which are also part of the FGSN network. Measurements are downloaded daily directly from GNSS receivers or FTP servers, analyzed and archived. Then high-precision coordinates of the stations are calculated and adjusted to the network of the International GNSS Service (IGS) in current implementations of the IGb20 reference frame [*Bakhtiarov and Zagretdinov*, 2021]. We processed GNSS measurements using the widely used in the scientific community Bernese GNSS software ver. 5.2 [*Bernese...*, 2015] developed by the Astronomical Institute (Bern). Our processing strategy closely follows the methodology established for Japan's GEONET, which comprises over 1,300 continuously operating reference stations (CORS) spaced at approximately 20 km intervals [*Takamatsu et al.*, 2023]. For calculating coordinates of stations in Kamchatka and Sakhalin during the period from July 28 to August 1, 2025, the Russian software InnoGNSS, developed at Innopolis University, was also used [*InnoGNSS*, 2025].

The availability of a sufficient number of GNSS stations in Kamchatka and Sakhalin with long measurement series allows for estimating tectonic movements of the Earth's surface in the region both before the extremely powerful July 29, 2025 earthquake in the Kamchatka region and during the subsequent period when numerous aftershocks were recorded.

The method of ionospheric radio sounding using signals from global navigation satellite systems (GNSS) has found wide application in studying various phenomena occurring in the Earth's ionosphere [*Pulinets and Boyarchuk*, 2005; *Yasukevich et al.*, 2013]. In particular, it is effectively used in research on the ionospheric response to earthquakes and the search for their precursors [*Pulinets and Boyarchuk*, 2005].

Using a set of GNSS data, as well as developed methodologies and software packages, this study investigates the crustal movements and ionospheric response to the main shock of the earthquake that occurred on July 29, 2025, in the Kamchatka Peninsula region with a magnitude of 8.8. This earthquake became the strongest seismic event in the world since the 2011 Tohoku earthquake of magnitude 9.1 off the coast of Japan and is the sixth most powerful earthquake ever recorded. Unlike Japan's dense GNSS network, the ionospheric response to seismic events in regions poorly covered by GNSS stations, such as Kamchatka, has been insufficiently studied.

2. Materials and Methods

2.1. GNSS Observations and Processing Methodology. Obtaining Time Series of Spatial Position Changes of GNSS Stations

2.1.1. GNSS Observation Processing Strategies

Currently, there are two main approaches to processing GNSS observations used for high-precision positioning: the Double Difference method and the Precise Point Positioning method. The relative double-difference method is used to obtain monitoring station coordinates relative to reference stations with known coordinates, while the Precise Point Positioning (PPP) method is used to determine coordinates relative to navigation satellites for which precise orbits and clock parameters are known [*Dach and the BSW-development team*, 2022; *InnoGNSS*, 2025; *Kaftan and Melnikov*, 2016; *Kaftan and Tatarinov*, 2021].

The data processing strategy involves two sequential stages. First, we employ the Bernese GNSS Software to perform PPP solutions for individual stations. This approach offers high computational efficiency through parallel processing capabilities, including the following steps:

- Standard PPP for coordinate, troposphere, and receiver clock determination
- Single- or multi-GNSS solutions (GPS, GLONASS, Galileo, BeiDou, QZSS)
- Ambiguity resolution, if consistent bias products are available
- Several extended processing options can be enabled: geocenter estimation, pseudo-kinematic, high-rate troposphere

At the second stage (F1 solution), the RNX2SNX double-difference network solution procedure may be used, which is efficient because clock parameters are not explicitly set up but requires bookkeeping to consider correlations due to differencing. This procedure includes:

- Standard double difference network solution
- Primary products are coordinates and troposphere corrections

- Single- or multi-GNSS solutions (GPS, GLONASS, Galileo, BeiDou, QZSS)
- Extended ambiguity resolution scheme
- Datum definition with verification based on minimum constraint solution

Global rates of changes in the coordinates of points (trends) were determined using the standard method of linear approximation by the least squares method. For time series longer than three years, the velocities in north-east components are determined with an accuracy of at least 0.1 mm/year. Periodic components of changes in coordinates were not determined.

For calculating coordinates of stations in Kamchatka and Sakhalin during the period from July 28 to August 1, 2025, the Russian software InnoGNSS, developed at the Innopolis University was also used. This software implements the Precise Point Positioning (PPP) method for processing satellite measurements, is included in the Unified Register of Russian Software for Electronic Computing Machines and Databases (https://reestr.digital.gov.ru/reestr/2643080/), and has been certified in the voluntary certification system for software of measuring instruments of the Federal State Budgetary Institution "All-Russian Research Institute of Metrological Service" (VNIIMS). During certification, coordinates obtained by InnoGNSS were compared with those obtained by reference software. It was found that the horizontal coordinate components agreed to within 0.5 cm, and the vertical coordinate component agreed to within 2.8 cm. InnoGNSS is available in a commercial full-function version and a freely distributed limited-function version. The limited-function version is available for download from the official website after signing a license agreement [*InnoGNSS*, 2025]. When using the InnoGNSS software, precise orbits and clock corrections from final CODE products were used. Processing of GPS and GLONASS radio signal measurements from 25 stations listed in Table 1 was performed using daily files.

Table 1. List of 25 used open GNSS stations in the Russian Far East region

Station name	Location	Lat. (°)	Lon. (°)	Height (m)	Plate	Start date	Network
41KL	Klyuchi	56.3182	160.8561	64.2	NOAM	2018-02-16	TopNET
41PT	Petropavlovsk-Kamchatsky	53.0356	158.6705	73.4	NOAM	2018-02-16	TopNET
65GK	Gor. Kluchi	52.0401	143.0795	36.6	EURA	2024-10-24	TopNET
65UG	Yuzhno-Sakhalinsk	46.9717	142.7004	71.2	EURA	2023-05-22	TopNET
ELIZ	Yelizovo	53.1804	158.3871	54.8	NOAM	2019-08-26	PRINNET
MGDN	Magadan	59.5663	150.8135	74.4	EURA	2024-02-27	PRINNET
NGLK	Nogliki	51.8108	143.1557	41.2	EURA	2023-12-12	PRINNET
OHAA	Okha	53.5695	142.9230	73.3	EURA	2023-11-23	PRINNET
ONOR	Onor	50.1875	142.6687	217.0	EURA	2024-11-27	PRINNET
PEMK	Petropavlovsk-Kamchatsky	53.0834	158.5911	209.7	EURA	2022-08-02	PRINNET
PONK	Poronaysk	49.2246	143.0955	33.7	EURA	2021-12-12	PRINNET
RDLN	Razdolnoe	46.6463	142.8102	58.2	EURA	2021-08-25	PRINNET
SAKH	Shakhtersk	49.1572	142.1118	81.2	EURA	2019-08-25	PRINNET
SKCH	Sokoch	53.1524	157.6913	353.2	EURA	2022-12-06	PRINNET
TMVS	Tymovskoe	50.8554	142.6623	141.8	EURA	2025-02-27	PRINNET
USKH	Yuzhno-Sakhalinsk	47.0350	142.7165	81.5	EURA	2019-11-20	PRINNET
VZMO	Vzmorie	47.8559	142.5041	50.9	EURA	N/A	PRINNET
ITRP	Iturup isl.	45.2536	147.8865	55.8	NOAM	2022-11-14	FAGN
KLCH	Kluchi	56.3246	160.8260	50.0	NOAM	2022-12-19	FAGN
MAG1	Magadan	59.5773	150.8104	74.5	EURA	2018-06-29	FAGN
OXTK	Okhotsk	59.3604	143.2348	19.7	EURA	2018-12-02	FAGN
PRVM	Pervomaisk	49.9602	143.2692	214.6	EURA	2022-09-21	FAGN
SVK1	Severo-Kurilsk	50.6663	156.1185	40.0	NOAM	2022-12-23	FAGN
SVK2	Severo-Kurilsk	50.6662	156.1185	45.9	NOAM	2022-12-22	FAGN
STK2	Shintotsukawa (Japan)	43.5286	141.8448	118.5	NOAM	2003-05-23	IGS

2.1.2. GNSS Stations in the Study Region

Approximately 40 continuously operating stationary GNSS stations with publicly available measurement data are currently active in the Russian Far East region. After considering the geographical location of these stations and selecting the most stable ones, we left 25 stations on the list for further analysis (Table 1). Seventeen stations belong to the FGSN network and 7 stations to the FAGN network. Since June 2022, access to data from IGS network stations MAG0, PETS, YSSK located in the Russian Federation has been discontinued. The nearest functioning IGS station to the region—STK2—is located in Japan (Figure 1). The specialized regional GNSS network KAMNET [*Shestakov et al.*, 2024] of Kamchatka Branch of the Geophysical Survey of the Russian Academy of Sciences provides GNSS measurements only for special requests. It should be noted that despite the discontinuation of the aforementioned IGS stations in the region, the five FAGN stations deployed in December of 2022 (Table 1), together with GNSS network stations of commercial operators belonging to the FGSN network, have enabled the acquisition of significant volumes of measurement information and the construction of time series of coordinate changes for these stations over at least a three-year interval. Table 2 presents a list of earthquakes with magnitudes greater than 6.5 that have occurred in the Russian Far East region since 2022.

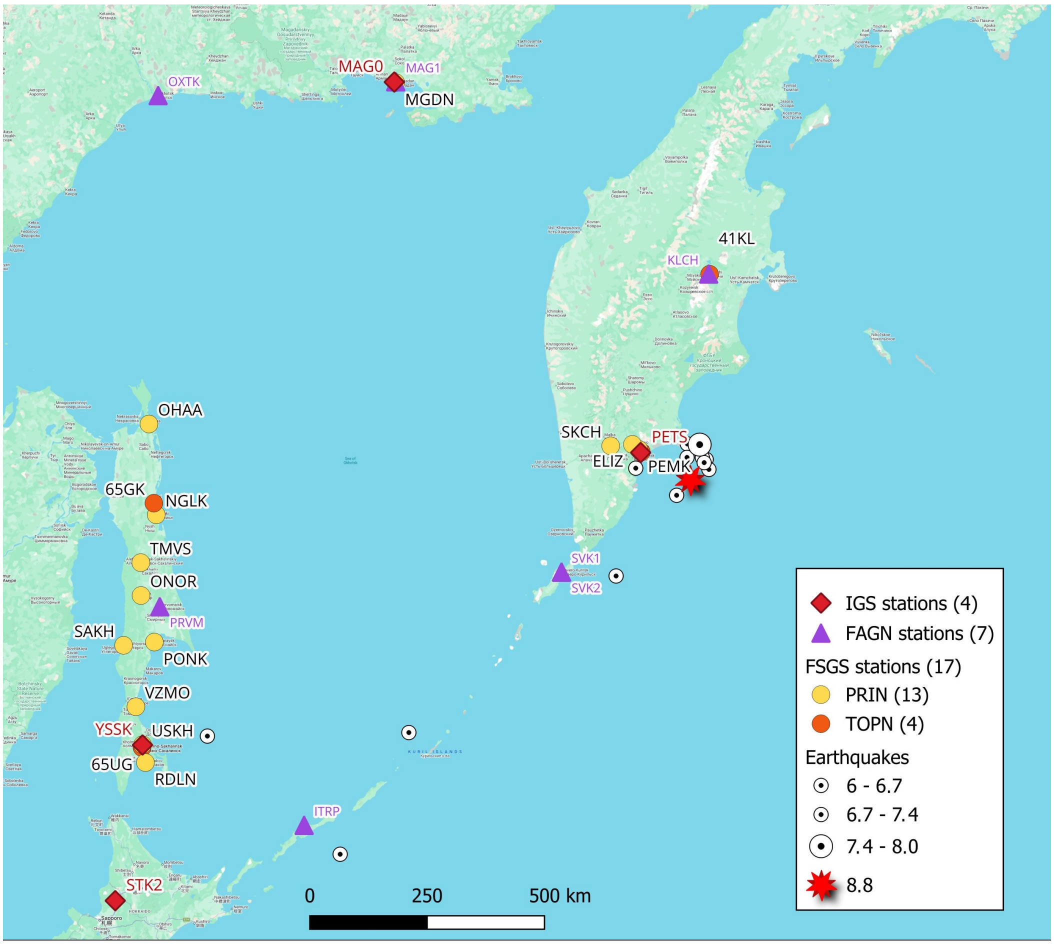

Figure 1. 25 permanent GNSS stations in the Russian Far East region and epicenters of earthquakes with magnitude greater than 6.0 since 2022.

Table 2. List of earthquakes with magnitude greater than 6.5 in the Russian Far East region since 2022 according to USGS data (https://earthquake.usgs.gov/earthquakes/search/).

No.	Time (UTC)	Lat. (°)	Lon. (°)	Depth (km)	Magnitude
1	2023-04-03T03:06:57.235Z	52.7227	158.4935	101	6.5
2	2023-12-28T09:15:16.131Z	44.596	149.0388	31	6.5
3	2024-08-10T03:28:32.681Z	47.223	144.7915	402.166	6.5
4	2024-08-17T19:10:26.820Z	52.9308	160.1331	29	7
5	2024-12-27T12:47:37.696Z	47.2996	151.236	146	6.8
6	2025-07-20T06:28:17.860Z	52.9286	160.6233	23	6.6
7	2025-07-20T06:49:04.327Z	52.8301	160.6816	34	7.4
8	2025-07-20T07:07:42.573Z	52.6981	160.8332	10	6.6
9	2025-07-20T07:23:02.065Z	52.8915	160.7461	34.991	6.5
10	2025-07-29T23:24:52.483Z	52.4948	160.2395	35	8.8
11	2025-07-30T00:09:58.961Z	52.1946	159.8008	36.622	6.9
12	2025-08-03T05:37:55.148Z	50.5853	157.8643	30	6.8
13	2025-09-13T02:37:56.847Z	53.1898	160.143	58.988	7.4
14	2025-09-18T18:58:15.240Z	53.1764	160.5373	29.998	7.8

2.2. Methodology for Investigating the Ionospheric Response to the Earthquake That Occurred on July 29, 2025 Based on GNSS Measurements

GNSS radio sounding enables determination of the spatial-temporal distribution of Total Electron Content (TEC) variations [*Saito et al.*, 1998] and related parameters such as ROT (Rate of TEC) and ROTI (Rate of TEC Index). This technique relies on the principle that each satellite-receiver line of sight (LOS) between a GNSS satellite and receiver provides a TEC measurement associated with a specific ionospheric pierce point (IPP) at any moment. Using data obtained from a dense network of GNSS stations, and plotting TEC variation values, color-coded according to the geographic position of the IPP for each LOS for all stations in the study region, TEC variation maps can be obtained with the time interval of the original GNSS data.

The original set of GNSS data consists of 30-second RINEX files. In total, the dataset contained more than 500 stations within a 5000 km radius from the epicenter. Of these, about 130 were from the KFU GNSS data archive, and more than 400 were from the SONEL (https://www.sonel.org/-GPS-.html), SOPAC/UNAVCO (http://garner.ucsd.edu/pub/), and Federal Navigation Data Center (https://fcnd.ru/datasearch/ftp_archive/) databases. The main stages of GNSS data processing were: 1) Extraction of phase measurements with time stamps from RINEX files; 2) Calculation of TEC, TEC variations, ROT and ROTI; 3) Mapping of the obtained TEC variations, ROT, and ROTI for IPPs at an altitude of 300 km with a data accumulation interval of 1 minute; 4) Calculation of median values of TEC variations for 3 sectors; 5) Construction of a distance–time diagram.

3. Results and Discussion

3.1. Time Series Analysis

Figure 2 displays the daily coordinate variations for station 41KL (Klyuchi) since 2023 after removing the global tectonic motions. The numbered markers in this figure correspond to the earthquake events listed in Table 2, with the July 29, 2025 M_W 8.8 Kamchatka earthquake causing the most significant displacements. It is clearly visible that earthquakes prior to July 29, 2025, practically did not cause significant movements of the Earth's surface at this station. The extremely powerful earthquake of July 29, 2025, at 23:24 UTC led to insignificant changes in north-east coordinates (15 mm). Significant changes in the height component of station 41KL were not observed.

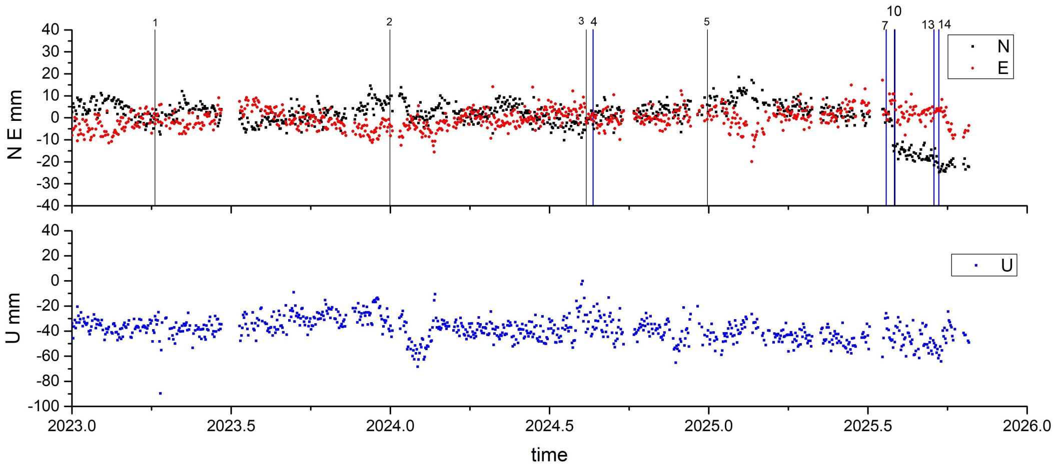

Figure 2. Horizontal (N E) and vertical displacements (U) at station 41KL since 2023. The vertical lines with numbers correspond to the times of past earthquakes in the region, according to Table 2. The vertical line with the number 10 corresponds to the extremely powerful earthquake on July 29, 2025.

Daily coordinate changes for stations ELIZ (Yelizovo) and 41PT (Petropavlovsk-Kamchatsky) after removing the global component are shown in Figures 3 and 4. Detailed analysis of the time series data for the 41PT GNSS station on the Kamchatka Peninsula shows that after the earthquake on July 20, 2025, at 06:49 UTC until July 29, 2025, at 23:24 UTC, the station shifted by 15 cm with an azimuth of 140°. After the main shock, the station shifted by 65.4 cm with an azimuth of 146°. The station continued to shift in the same direction until the September 13, 2025, at 02:37 UTC magnitude 7.4 shock. The shift in the north-east direction over 44 days was up to 12 cm. Similar displacement characteristics are observed for the ELIZ station (Figure 3).

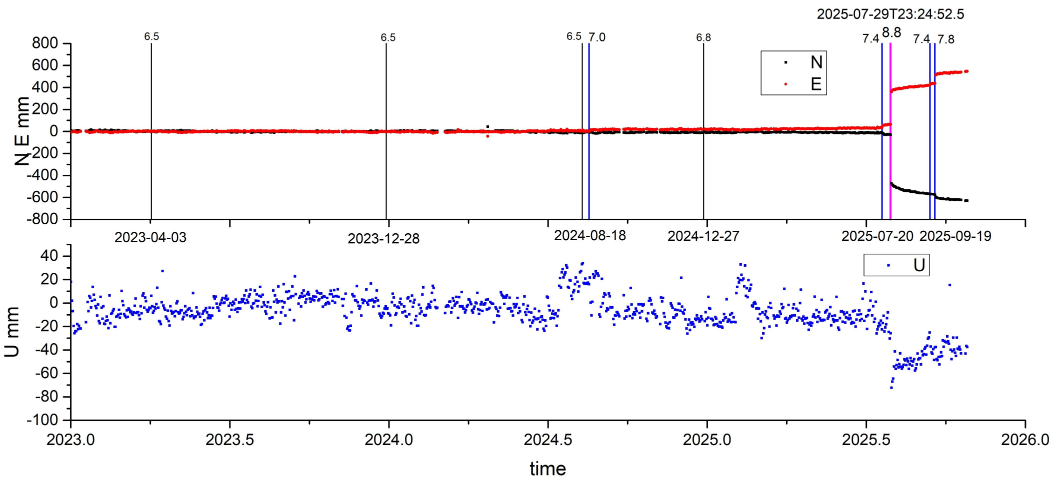

Figure 3. Horizontal (N E) and vertical displacements (U) at station ELIZ since 2023. The magnitude of the earthquakes is listed above the vertical lines, and the date is listed below. The magenta vertical line with magnitude 8.8 corresponds to the extremely powerful earthquake on July 29, 2025 at 23:24 UTC.

Stations SVK1 and SVK2 in Severo-Kurilsk are located within a few meters of each other but have different antenna and GNSS receiver models. Therefore, the daily coordinate changes for stations SVK1 and SVK2 shown in Figure 5 practically coincide. Detailed analysis of the time series data for the SVK1 and SVK2 stations shows that there were no significant displacements of both stations after the earthquake of July 20, 2025, at 06:49 UTC until July 29, 2025, at 23:24 UTC. After the main shock, the stations shifted in

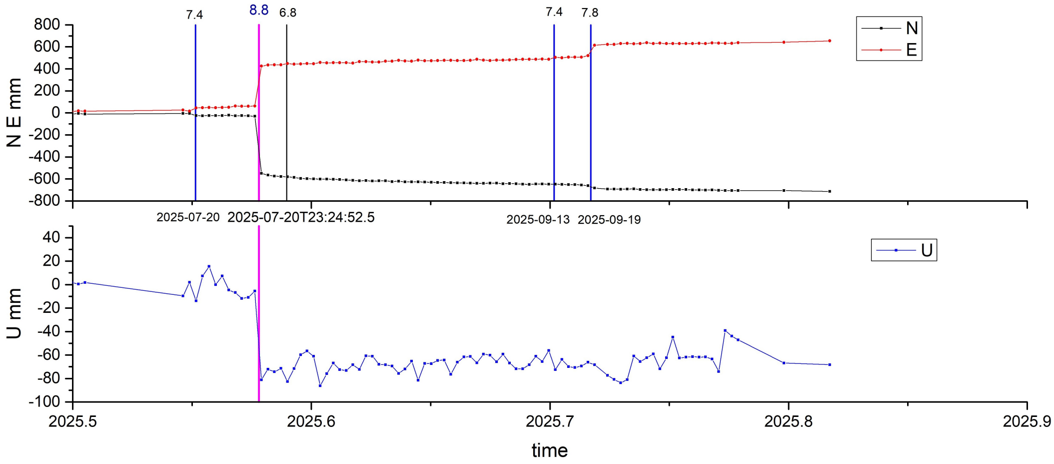

Figure 4. Horizontal (N E) and vertical displacements (U) at station 41PT since mid-2025. The magnitude of the earthquakes is listed above the vertical lines, and the date is listed below. The magenta vertical line with magnitude 8.8 corresponds to the extremely powerful earthquake on July 29, 2025 at 23:24 UTC.

the north-east by 1.693 m (SVK1) and 1.683 m (SVK2) with an azimuth of 120°. The height component for SVK1 and SVK2 decreased simultaneously by 19 cm. Stations SVK1 and SVK2 continued to shift in the same direction until the aftershock of September 13, 2025, at 02:37 UTC (event 13) with a magnitude of 7.4. The horizontal displacement of the stations was 9 cm in 44 days. After this quake and the magnitude 7.8 aftershock that immediately followed, the displacement of stations continued. Thus, for the period from July 20 to September 18, 2025, the total displacement of stations SVK1 and SVK2 was about 1.78 m with an azimuth of about 120°.

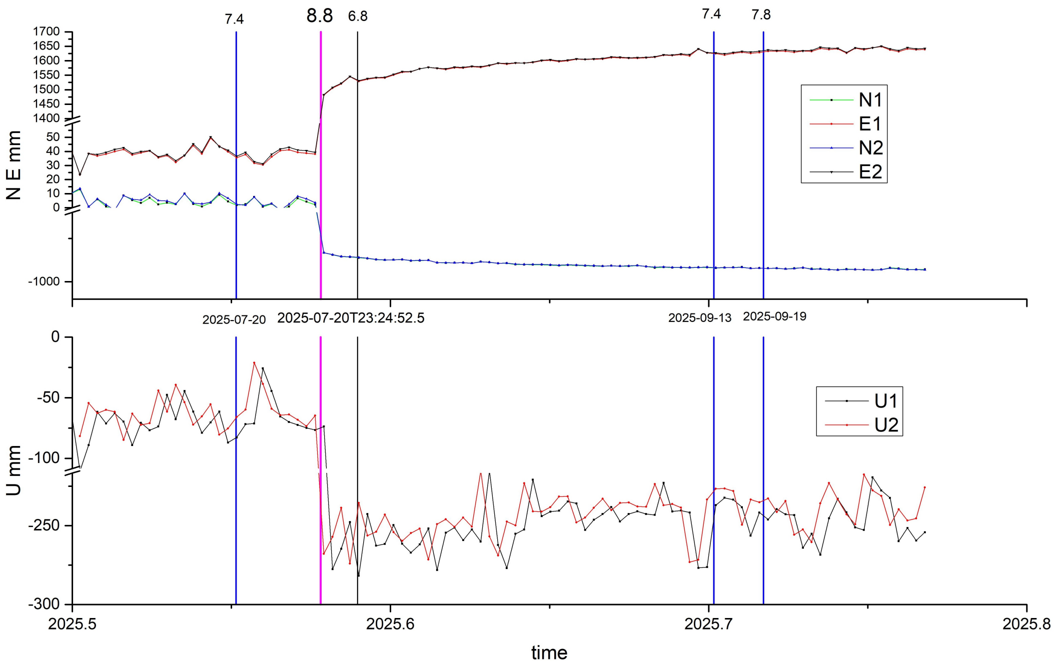

Figure 5. Daily solutions in 2025 for SVK1 horizontal (N1 E1) and vertical displacements (U1) and for SVK2 horizontal (N2 E2) and vertical displacements (U2) stations at Severo-Kurilsk. The magnitude of the earthquakes is listed above the vertical lines, and the date is listed below. The magenta vertical line with magnitude 8.8 corresponds to the extremely powerful earthquake on July 29, 2025 at 23:24 UTC.

Analysis of high-frequency GNSS measurements is of particular interest, as it allows determination of second-by-second coordinate changes using PPP technology [*Banville et al.*, 2020]. Such a service is implemented by the Canadian Geodetic Survey (https://natural-resources.canada.ca/maps-tools-publications/data). Figure 6 shows coordinate changes from July 29 to 30, 2025, for station 41PT (Petropavlovsk-Kamchatsky). After the moment of the main shock of magnitude 8.8 that occurred at 23:24:52.483 UTC, significant changes in north-east and height components of the station began approximately 45 seconds later. For station SVK1 (Severo-Kurilsk), this time delay was about 123 seconds (Figure 7). This station exhibited the most significant displacements of the Earth's surface, the detailed analysis of which is still pending.

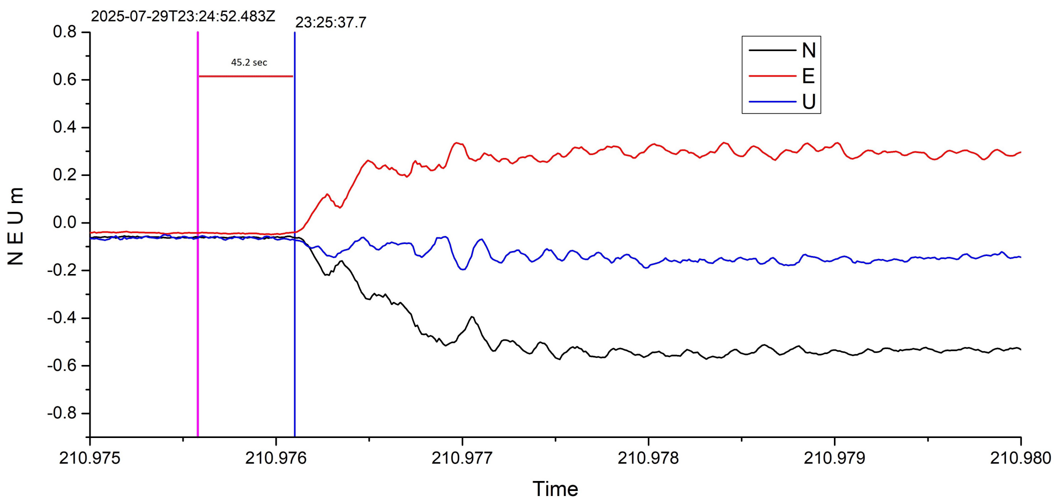

Figure 6. 1-second kinematic solutions July 29, 2025 (210 day of the year), 41PT in Petropavlovsk-Kamchatsky. North – black line, East – red line, Up – blue line. The magenta vertical line corresponds to the extremely powerful earthquake on July 29, 2025 at 23:24 UTC. The blue vertical line corresponds to moment when significant displacements of the Earth's surface began.

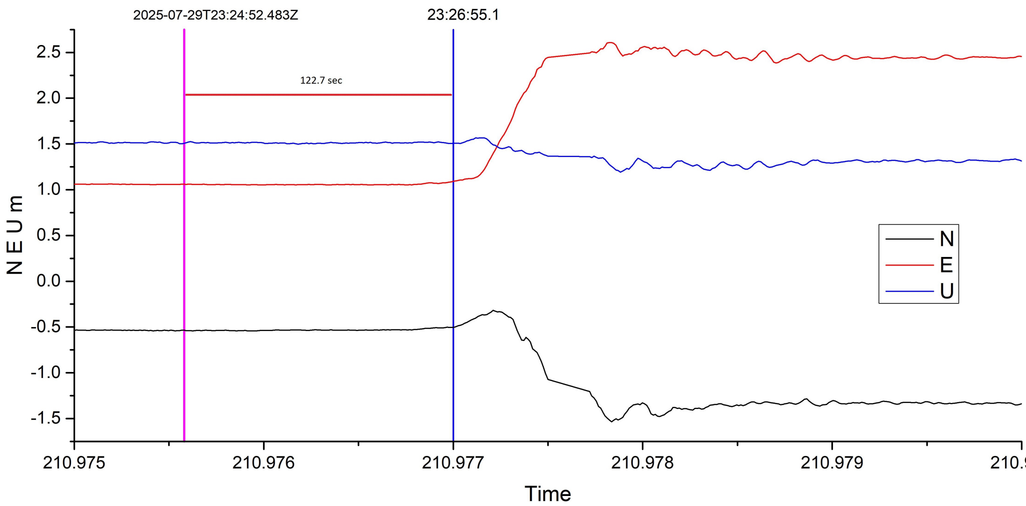

Figure 7. 1-second kinematic solutions July 29, 2025 (210 day of the year), SVK1 in Severo-Kurilsk. North – black line, East – red line, Up – green line. The magenta vertical line corresponds to the extremely powerful earthquake on July 29, 2025 at 23:24 UTC. The blue vertical line corresponds to moment when significant displacements of the Earth's surface begun.

Similar studies have been conducted at several stations of the KAMNET network and impressive animations of fast movements have been created and presented on the Telegram channel of the Kamchatka branch of the Geophysical Survey of the Russian Academy of Sciences (https://t.me/kbgsras).

At the moment of the earthquake wave arrival at station SVK1, the GNSS receiver recorded a triple decrease in the number of satellites (NSV) used in the solution (Figure 8). Additionally, the Geometric Dilution Of Precision (GDOP) parameter of satellite constellation geometry significantly increased at the receiver.

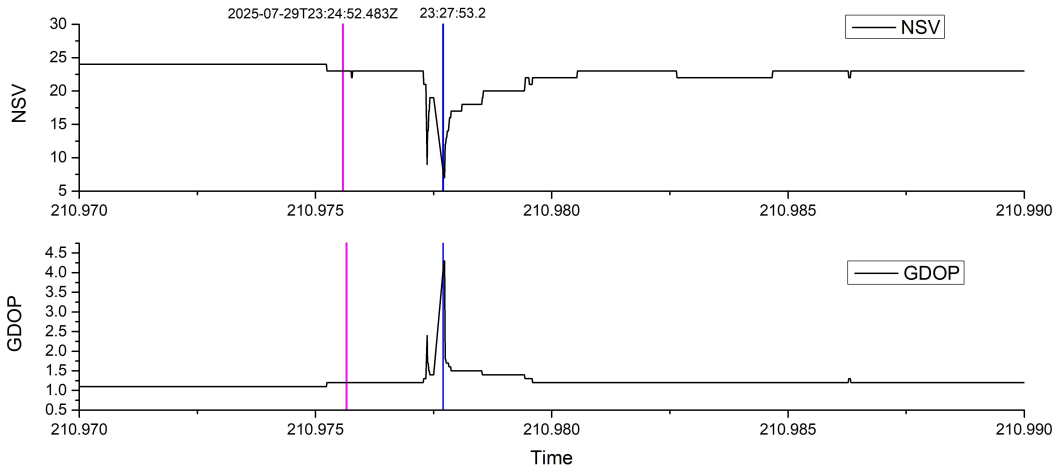

Figure 8. GDOP and NSV July 29, 2025 (210 day of the year) for SVK1 station in Severo-Kurilsk. The magenta vertical line corresponds to the extremely powerful earthquake on July 29, 2025 at 23:24 UTC. The blue vertical line corresponds to moment when the number of satellites in use has greatly decreased and geometry of the satellite constellation has deteriorated significantly.

For further analysis of changes between GNSS station positions before and after the earthquake, the displacements were presented in a topocentric coordinate system and are shown in Table 3. Graphs of coordinate changes from July 28 to August 1, 2025, for 25 stations are presented in Figure 9.

As can be seen from the table, displacements occurred in the southeast direction with azimuths of 120°–146°. The largest horizontal displacement occurred at stations SVK1 and SVK2 (Severo-Kurilsk, Paramushir Island) and amounted to approximately 1.7 m. Smaller displacements are noticeable at the northern part of the Kamchatka Peninsula. In other places, no significant displacements were detected.

It is noteworthy that vertical displacements are significantly smaller than horizontal ones and do not exceed 0.19 m. The displacement vector values and their directions for the processed GNSS stations are shown in Figure 10.

3.2. Assessment of Ionospheric Response to the July 29, 2025 Earthquake Based on GNSS Measurements

By mapping vertical TEC variations at each time moment according to the geographic coordinates of the corresponding IPP and color-coding the amplitude intensity, we generated spatiotemporal maps of TEC variation distribution. Figure 11 displays the temporal evolution of these maps for July 29, 2025, in the interval 23:20–23:55 UTC with a 5-minute time step. Deviations of TEC variations from the background (undisturbed) level—represented by green dots—are displayed in red for positive deviations and in blue for negative deviations, revealing the propagation pattern of ionospheric disturbances triggered by the main earthquake shock.

Analysis of the dynamics of TEC variation presented in Figure 11 revealed concentric ionospheric disturbances propagating from the earthquake epicenter. Pronounced TEC perturbations were recorded from 23:35 to 23:55 UTC, with amplitudes reaching ~0.2 TECU and greater. The disturbances propagated predominantly southwestward, as clearly visible on the TEC maps at 23:40 and 23:45 UTC. These maps show a sharp increase in TEC variation intensity (red and blue dots relative to background level), forming a V-shaped

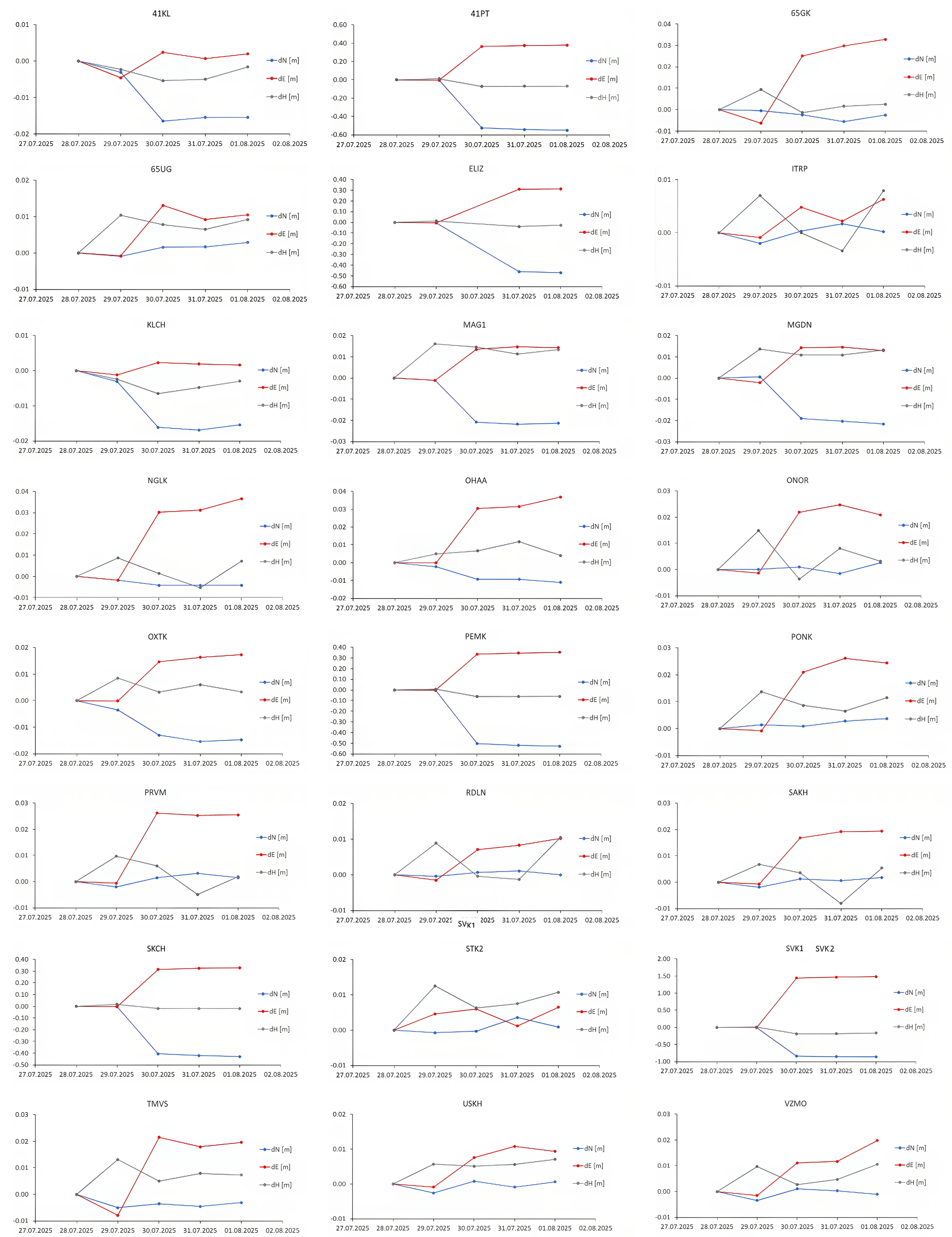

Figure 9. Coordinate changes from July 28 to August 1, 2025, for 25 stations listed in Table 1.

structure that attenuated with distance and became undetectable beyond approximately 1250 km from the earthquake epicenter. It should be noted that this direction is the most densely covered by GNSS receivers; however, weaker responses are visible from the north-west or north-east directions based on available data.

As seen in Figure 12, the first disturbances in the TEC variation series (first minimum at 23:27 UTC, -0.015 TECU) were recorded 3 minutes after the onset of the main shock (magnitude 8.8, 23:24 UTC). Based on the maximum values of the median TEC variations shown in Figure 12 right panel, the time difference between the maximum TEC variations in the first (black) sector and the second (red) sector was approximately 6 minutes. Thus, the disturbances propagate at a velocity of approximately 900 m/s. From the first sector to the third, the distance between maximum values is 8 minutes, corresponding to a velocity

Table 3. GNSS station displacements in the period from July 28 to August 1, 2025 for 25 stations in the Far Eastern region listed in Table 1.

Name	sN (m)	sE (m)	sH (m)	sHz (m)	Az (°)
41KL	-0.014	0.004	-0.003	0.015	66
41PT	**-0.537**	**0.373**	**-0.076**	**0.654**	**146**
65GK	-0.003	0.032	-0.004	0.033	78
65UG	0.003	0.011	0.003	0.012	93
ELIZ	**-0.463**	**0.314**	**-0.039**	**0.559**	**151**
ITRP	0.002	0.005	-0.002	0.005	40
KLCH	-0.015	0.003	-0.004	0.015	45
MAG1	-0.021	0.015	0.005	0.025	130
MGDN	-0.021	0.015	0.005	0.025	147
NGLK	-0.003	0.034	-0.003	0.034	107
OHAA	-0.009	0.033	0.005	0.034	90
ONOR	0.001	0.023	-0.005	0.023	67
OXTK	-0.013	0.016	0.000	0.020	123
PEMK	**-0.514**	**0.345**	**-0.065**	**0.619**	**149**
PONK	0.002	0.024	0.002	0.024	107
PRVM	0.003	0.026	-0.004	0.026	16
RDLN	0.001	0.009	-0.002	0.009	85
SAKH	0.002	0.019	-0.003	0.019	62
SKCH	**-0.417**	**0.325**	**-0.028**	**0.528**	**145**
STK2	0.002	0.002	0.002	0.003	138
SVK1	**-0.848**	**1.465**	**-0.182**	**1.693**	**120**
SVK2	**-0.841**	**1.458**	**-0.194**	**1.683**	**121**
TMVS	-0.001	0.024	0.000	0.024	72
USKH	0.001	0.010	0.003	0.010	69
VZMO	0.002	0.015	0.001	0.015	109

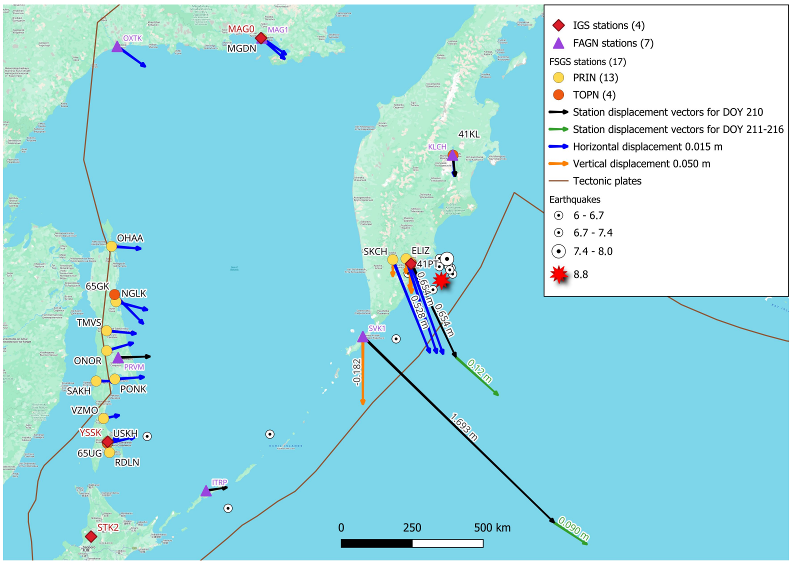

Figure 10. Displacement vector values and their directions for 25 stations in the Far Eastern region listed in Table 3.

of approximately 1350 m/s at a distance of about 350 km between sectors. It should be noted that significant data scatter within sectors 1 and 2 (Figure 12) reduces the accuracy of determining the timing of extrema and, consequently, the calculation of velocities.

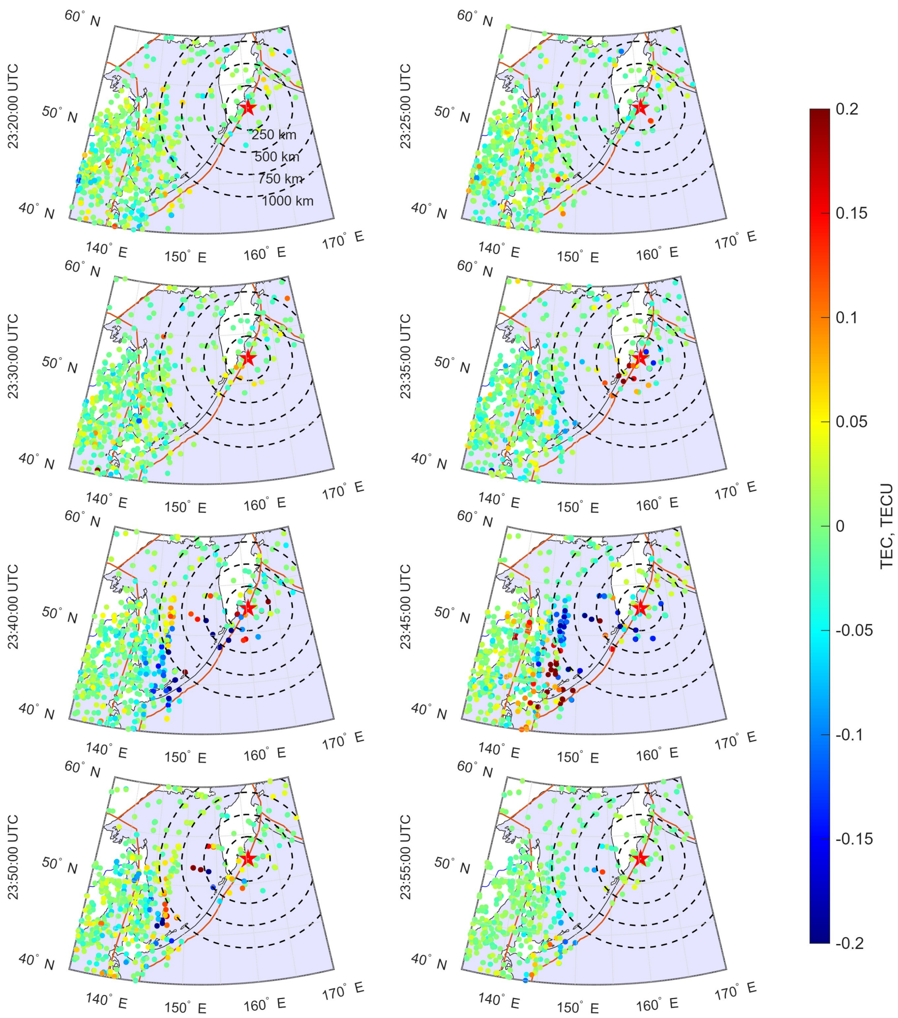

Figure 11. Dynamics of TEC variation maps on July 29, 2025, in the interval 23:20–23:55 UTC. TEC variation values (in TECU) are displayed as dots, with intensity represented by color-coding. Black dotted circles show distance from the earthquake epicenter (red star marker) with a step of 250 km.

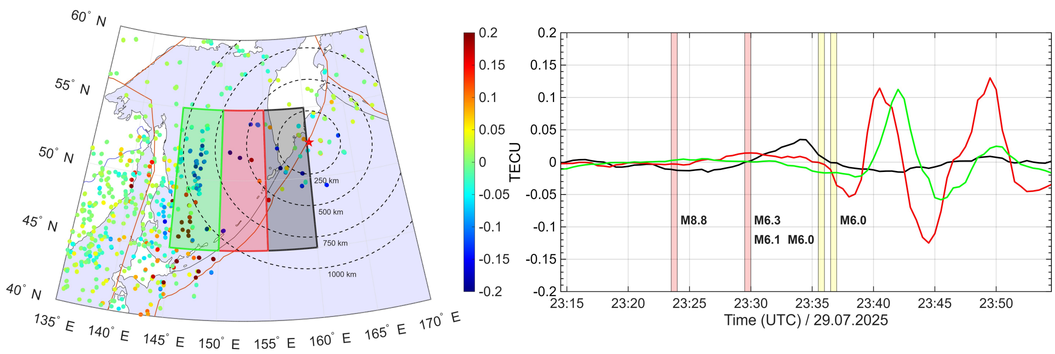

Figure 12. Dynamics of median TEC values by separate sectors. Left: TEC variation map for 23:45 UTC July 29, 2025, with three highlighted sectors. Right: Changes in intensity of median TEC variation values for the corresponding sector. Colors of sectors on the left correspond to the color of the intensity line in the right figure. Red and yellow vertical bands indicate earthquakes with corresponding magnitudes.

Another effective way to estimate the propagation velocity of the disturbance is to construct a distance–time diagram [*Calais et al.*, 2003], where the observed value of TEC variations is correlated with the registration time and distance to the earthquake epicenter.

By calculating the distance from each IPP to the earthquake epicenter and color-coding the TEC variation value, a two-dimensional map of TEC variations is obtained in the time-distance coordinate system. The slope of the line, or lines in the case of a multi-mode disturbance on such a map, can be used to calculate the propagation velocities of disturbances.

The distance–time diagram obtained in the interval July 29, 2025, 23:00 UTC – July 30, 2025, 01:30 UTC, presented in Figure 13, clearly confirms the conclusion about the propagation of wave disturbances from the epicenter, drawn from the dynamics of median TEC values in three sectors (see Figure 12). The observed inclined lines, whose vertices converge to the moment and place of the main shock, correspond to different phase velocities. Quantitative analysis of the line slopes allows identification of two phases of propagation: an initial fast phase with a velocity of 800–1300 m/s during the first ~20 minutes, and a subsequent slow phase with a velocity of 180–330 m/s, observed approximately 40 minutes after the shock. Such a sharp decrease in velocity is a sign of atmospheric gravity wave (AGW) dispersion, where the fast phase corresponds to the acoustic mode, and the slow phase to the internal gravity mode. The decrease in amplitude and "blurring" of structures over time indicates wave damping and, possibly, interference of different modes.

Considering the small number of GNSS stations in the study region, especially in the area immediately adjacent to the earthquake epicenter, the detail of the TEC variation maps (Figure 11) and the distance–time diagram (Figure 13) does not allow for a detailed assessment of the fine structure of the ionospheric response to this event, similar to previously obtained results from studies of the 2011 Tohoku earthquake in Japan [*Astafyeva et al.*, 2011; *Heki*, 2011; *Kunitsyn et al.*, 2011; *Tsugawa et al.*, 2011]. Japan's GNSS network has a significantly higher station density, which allowed obtaining more detailed TEC maps, more fully assessing the propagation vector of the disturbance, clearly identifying several transfer modes of the ionospheric disturbance on the distance–time diagram, areas with heterogeneous spatial structure of TEC variations, and other post-effects.

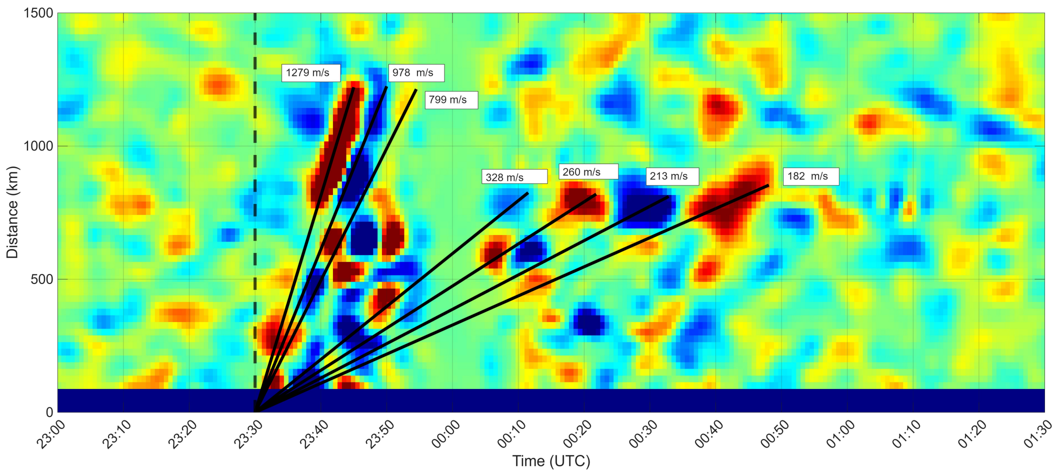

Figure 13. Distance–time diagram of the TEC variations in the interval July 29, 2025, 23:00 UTC - July 30, 2025, 01:30 UTC. The dotted vertical line marks the moment of the main shock.

It should be noted that in the study region, only 28 GNSS stations are located within a 1000 km radius from the earthquake epicenter, and 65 GNSS stations were within a radius of approximately 1500 km, indicating extremely low coverage of this highly seismically active region by stationary GNSS stations. The predominant direction of propagation of the recorded disturbance from the main earthquake shock is southwest; however, it is precisely in this direction that the overwhelming number of stations are located, and we were unable to fully assess other directions of propagation due to the reasons described above. The obtained velocities of 800–1300 m/s and 180–330 m/s are consistent with the velocities of acoustic and gravity modes of AGW observed during other strong earthquakes, for example, during the 2011 Tohoku earthquake in Japan [*Astafyeva et al.*, 2011; *Tsugawa et al.*, 2011], where similar structures of circular and concentric waves with several modes from 3000 m/s in the initial phase at the moment of rupture, 1300–1500 m/s in the main phase of disturbance propagation from the rupture, and later waves with velocities of 180–423 m/s were recorded. These works also showed that the propagation velocities of disturbances tended to decrease over time.

The sparse GNSS station coverage across this region significantly limits our ability to fully reconstruct the detailed structure of the ionospheric response. This limited spatial resolution prevents us from identifying finer features and asymmetries that would likely be apparent with denser monitoring infrastructure comparable to Japan's GEONET. Currently, there is a large number of GNSS modules and development boards based on them available on the commercial market for small scientific groups, supporting reception of all operational GNSS signals with a 1-second interval and providing acceptable data quality for solving problems of studying ionospheric disturbances using the method of ionospheric radio sounding [*Kogogin et al.*, 2023].

4. Conclusion

The analysis of high-frequency GNSS measurements made it possible to determine the second-by-second changes in the coordinates of GNSS stations and estimate the propagation time of the seismic wave from the earthquake epicenter to stations 41PT (Kamchatka Peninsula) and SVK1 (the Kuril Islands). After the moment of the main shock with a magnitude of 8.8, which occurred on July 29, 2025, at 23:24:52.483 UTC, significant changes in the north-east coordinates and height component of the 41PT station began approximately 45 seconds later. For SVK1 station, this delay was about 123 seconds. For the period from July 20 to September 18, 2025, the total displacement of stations SVK1 and SVK2 was about 1.78 m with an azimuth of about 120°. For the 41PT GNSS station, the shift in the north-east direction over 44 days was 12 cm.

The analysis of GNSS data reveals two distinct phases of ionospheric disturbance propagation. The initial fast mode (800–1300 m/s) was observed during the first ~20 minutes, and the slower mode (180–330 m/s), approximately 40 minutes after the shock. The observed inclined lines on the distance-time diagram converge toward the time and location of the main earthquake epicenter. The concentric ionospheric disturbances we detected, propagating from the earthquake epicenter primarily in the southwest direction, exhibited a pattern similar to those observed following the 2011 Tohoku earthquake in Japan. However, the sparse GNSS station coverage across this region significantly limits our ability to fully reconstruct the detailed structure of the ionospheric response.

Future deployment of dense GNSS networks across the Kamchatka Peninsula would enable more comprehensive monitoring of both seismic displacements and associated ionospheric effects, ultimately improving our understanding of earthquake-ionosphere relationships and potentially contributing to multi-parameter earthquake forecasting systems.

Acknowledgments. The authors sincerely thank the Center for Geodesy, Cartography, and Spatial Data Infrastructure of PLC "Roskadastr", companies JSC "PRIN" (PRINNET), LLC "GEOSTROYIZYSKANIYA" (TopNETlive), LLC "Smartnet Geosystems" (SmartNet), SONEL and SOPAC/UNAVCO centers, and the Federal Navigation Data Center for the open GNSS data used in this work. The study of the ionospheric response to the earthquake was supported by the grant from the Russian Science Foundation No. 23-77-10029, https://rscf.ru/project/23-77-10029/.

References

Astafyeva E., Lognonné P. and Rolland L. M. First ionospheric images of the seismic fault slip on the example of the Tohoku-oki earthquake // Geophysical Research Letters. — 2011. — Vol. 38, no. 22. — P. L22104. — https://doi.org/10.1029/2011gl049623

Bakhtiarov V. F. and Zagretdinov R. V. On geodynamics of continuously operating stationary GNSS stations in the territory of the Russian Federation // Geoprofi. — 2021. — No. 1. — P. 34–37. — (In Russian).

Banville S., Geng J., Loyer S., et al. On the interoperability of IGS products for precise point positioning with ambiguity resolution // Journal of Geodesy. — 2020. — Vol. 94, no. 1. — https://doi.org/10.1007/s00190-019-01335-w

Bernese GNSS Software Version 5.2 / ed. by R. Dach, S. Lutz, P. Walser, et al. — University of Bern, 2015. — 826 p. — https://doi.org/10.7892/BORIS.72297

Calais E., Haase J. S. and Minster J. B. Detection of ionospheric perturbations using a dense GPS array in Southern California // Geophysical Research Letters. — 2003. — Vol. 30, no. 12. — https://doi.org/10.1029/2003gl017708

Dach R. and the BSW-development team. Spotlight on Bernese GNSS Software // Technical Seminar, 10-11 Sept. 2022. — Warsaw, Poland : FIG, 2022.

Heki K. Ionospheric electron enhancement preceding the 2011 Tohoku-Oki earthquake // Geophysical Research Letters. — 2011. — Vol. 38, no. 17. — P. L17312. — https://doi.org/10.1029/2011gl047908

InnoGNSS. Software for high-precision processing of static measurements of radio signals of global navigation satellite systems. — URL: https://rnd.innopolis.university/projects/programmnoe-obespechenie-dlya-vysokotochnoy-obrabotki-staticheskikh-izmereniy-radiosignalov-globalny/ (visited on 11/11/2025) ; (in Russian).

Kaftan V. and Melnikov A. Deformation precursors of large earthquakes derived from long term GNSS observation data // Russian Journal of Earth Sciences. — 2016. — Vol. 16. — ES3001. — https://doi.org/10.2205/2016ES000568

Kaftan V. and Tatarinov V. An Analysis of Possibilities of GNSS Local Strain Monitoring Networks in Earthquake-Prone Areas // Journal of Volcanology and Seismology. — 2021. — Vol. 15, no. 6. — P. 379–386. — https://doi.org/10.1134/s074204632106004x

Kogogin D. A., Sokolov A. V., Nasirov I. A., et al. Signal Receiver for Global Navigation Satellite Systems Based on a U-Blox ZED-F9P Module for Ionospheric Research // Journal of Communications Technology and Electronics. — 2023. — Vol. 68, no. 6. — P. 682–691. — https://doi.org/10.1134/s1064226923060074

Kunitsyn V. E., Nesterov I. A. and Shalimov S. L. Japan megathrust earthquake on March 11, 2011: GPS-TEC evidence for ionospheric disturbances // JETP Letters. — 2011. — Vol. 94, no. 8. — P. 616–620. — https://doi.org/10.1134/s0021364011200082

Lapshin A. and Staroverov S. Creation and development of continuously operating networks in the Russian Federation. Yesterday, today, tomorrow // FIG Working Week 2024. — Accra, Ghana : FIG, 2024.

Pulinets S. A. and Boyarchuk K. A. Ionospheric precursors of earthquakes. — Berlin : Springer-Verlag, 2005. — 315 p. — https://doi.org/10.1007/b137616

Saito A., Fukao S. and Miyazaki S. High resolution mapping of TEC perturbations with the GSI GPS Network over Japan // Geophysical Research Letters. — 1998. — Vol. 25, no. 16. — P. 3079–3082. — https://doi.org/10.1029/98gl52361

Shestakov N. V., Nechaev G. V., Titkov N. N., et al. GNSS-Based Modeling and Study of Postseismic Crustal Movement of the May 24, 2013, MW 8.3 Sea of Okhotsk Deep-Focus Earthquake // Geodynamics & Tectonophysics. — 2024. — Vol. 15, no. 3. — P. 0761. — https://doi.org/10.5800/gt-2024-15-3-0761

Takamatsu N., Muramatsu H., Abe S., et al. New GEONET analysis strategy at GSI: daily coordinates of over 1300 GNSS CORS in Japan throughout the last quarter century // Earth, Planets and Space. — 2023. — Vol. 75, no. 1. — https://doi.org/10.1186/s40623-023-01787-7

Tsugawa T., Saito A., Otsuka Y., et al. Ionospheric disturbances detected by GPS total electron content observation after the 2011 off the Pacific coast of Tohoku Earthquake // Earth, Planets and Space. — 2011. — Vol. 63, no. 7. — P. 875–879. — https://doi.org/10.5047/eps.2011.06.035

Yasukevich Yu. V., Perevalova N. P., Edemskiy I. K., et al. Ionospheric response to helio- and geophysical disturbing factors based on GPS data. — Irkutsk : ISU Publ., 2013. — 259 p. — (In Russian).